Asian Journal of Chemistry; Vol. 38, No. 5 (2026), 1212-1220

ASIAN JOURNAL OF CHEMISTRY

https://doi.org/10.14233/ajchem.2026.35079

Molecular Design and Characterisation of Hyaluronic Acid-Based Nanogel Sponges for Controlled Glutathione Release and Wound Healing

SNEHA PANNEERSELVAM, SAFIQ HUSSAIN JAHIR, LISHA KUMAR, KIRUTHIKA GANESAN and RENUKADEVI JEYAVELKUMARAN*

Department of Pharmaceutics, Saveetha College of Pharmacy, Saveetha Institute of Medical and Technical Sciences, Chennai-602105, India

*Corresponding author: E-mail: neelarenu@gmail.com

Received: 16 October 2025 *Accepted*: 19 March 2026 *Published online*: 4 May 2026 AJC-22346

The development of sustainable, bio-based polymeric materials with controlled release functionality is of growing interest for advanced wound-healing applications. In this study, a hyaluronic acid (HA) based nanogel sponge scaffold incorporating glutathione (GSH) loaded chitosan nanogels was rationally designed using ionic gelation followed by freeze-drying. This green and mild fabrication strategy enabled the stabilisation of the redox-active thiol functionality of GSH while generating a hierarchically porous HA sponge architecture. Comprehensive physico-chemical characterisation using UV-diffuse reflectance spectroscopy, FTIR, differential scanning calorimetry, zeta potential analysis, dynamic light scattering, scanning electron microscopy and transmission electron microscopy confirmed successful molecular integration, preservation of functional groups, nanoscale uniformity, interconnected porosity and satisfactory thermal and colloidal stability. The scaffold exhibited a controlled, diffusion-driven swelling profile, supporting sustained moisture retention under simulated wound conditions. *In vitro* anti-inflammatory evaluation demonstrated concentration-dependent inhibition of bovine serum albumin and egg albumin denaturation, along with significant red blood cell membrane stabilisation, with higher concentrations approaching the activity of the reference drug. These findings demonstrate that HA-GSH nanogel sponges represent a sustainably engineered, redox-responsive polymer system capable of providing structural support, controlled molecular release and anti-inflammatory functionality. This study contributes to the advancement of bio-based polysaccharide materials and green nanogel synthesis related to health, responsible production and materials innovation.

Keywords: Biopolysaccharides, Green nanogel, Redox-responsive polymers, Hierarchical materials, Controlled molecular release.

INTRODUCTION

The rational design of multifunctional polymeric materials has become a central focus in contemporary materials chemistry, particularly for systems that integrate molecular stabilisation, controlled release and hierarchical structural organisation [1]. Among natural polysaccharides, hyaluronic acid (HA) has attracted significant attention due to its well-defined chemical structure, high density of hydroxyl and carboxylate groups and strong hydration capability arising from extensive hydrogen-bonding networks [2]. These features make HA an attractive platform for constructing chemically tunable soft materials such as hydrogels, nanogels and porous sponges. However, from a molecular chemistry perspective, native HA lacks intrinsic redox-active functionality, limiting its applicability in systems where oxidative stability and chemical protection of labile molecules are required.

Glutathione (GSH) is a low-molecular weight tripeptide characterised by a reactive thiol (–SH) group, which plays a critical role in redox chemistry through reversible oxidation–reduction reactions [3]. The high nucleophilicity and oxidation sensitivity of the thiol group, however, present significant challenges in material integration, as GSH readily undergoes oxidative degradation in aqueous and oxygen-rich environments. From a chemical standpoint, effective incorporation of GSH into polymeric matrices therefore requires strategies that minimize thiol oxidation while maintaining molecular accessibility and release controllability [4]. Recent advances in the peptide engineering have highlighted the importance of overcoming biological barriers such as epithelial permeability, enzymatic degradation and controlled transport, emphasizing the need for biomaterial systems that can modulate barrier interactions while preserving bioactivity [5]. Nanogel chemistry offers a versatile approach for addressing these challenges.

Chitosan-based nanogels, formed *via* ionic gelation, exploit electrostatic interactions between protonated amine groups and multivalent counterions to generate nanoscale polymer networks without the need for harsh chemical crosslinkers [6]. This mild synthesis route is particularly advantageous for encapsulating redox-sensitive molecules such as GSH, as it preserves molecular integrity while enabling spatial confinement at the nanoscale [7]. The resulting nanogels function as chemically protective microenvironments, reducing thiol exposure to external oxidants and allowing diffusion-controlled release governed by polymer relaxation and hydration dynamics. Embedding such nanogels within a macroscopic polymer scaffold introduces an additional level of structural hierarchy. Freeze-dried HA sponges represent a chemically driven architecture in which ice-templated phase separation generates interconnected pore networks with high surface area and tunable porosity [8].

From a materials chemistry perspective, this approach enables simultaneous control over molecular interactions at the nanometer scale and mass-transport behaviour at the micrometer scale. The integration of GSH-loaded chitosan nanogels into an HA sponge matrix therefore creates a composite system in which hydrogen bonding, electrostatic interactions and thiol chemistry collectively govern stability, swelling and release behaviour. Despite increasing interest in HA-based hydrogels and nanogel systems, systematic studies that correlate molecular-level interactions, thermal behaviour, colloidal properties and hierarchical morphology in HA-GSH composite sponges remain limited [9]. Recent studies on electrospun HA-GSH-PVA nanofiber scaffolds have further demonstrated enhanced fibroblast migration and accelerated wound healing, highlighting the therapeutic relevance of HA-GSH composite systems in tissue regeneration [10]. In particular, there is limited chemistry-focused research explaining the effect of nanogel incorporation on polymer–polymer compatibility, thermal transitions, optical response, and swelling kinetics in freeze-dried HA matrices. In this work, hyaluronic acid based nano-gel sponge scaffolds incorporating GSH-loaded chitosan nanogels were developed using ionic gelation followed by freeze-drying to obtain a hierarchical composite material. The physico-chemical characterization using UV-DRS, FTIR, DSC, zeta potential, DLS, SEM, and TEM was performed to establish structure–property relationships. The Swelling and stability studies were conducted to understand solvent-polymer inter-actions and network relaxation. The results demonstrate that HA-GSH nanogel sponges' function as chemically engineered polymeric materials with controlled redox functionality and tunable structural properties.

EXPERIMENTAL

Chitosan (medium molecular weight) was used as primary polymer for nanogel formation, while reduced glutathione (GSH) served as the entrapped antioxidant molecule. Sodium tripolyphosphate (TPP) was employed as the ionic crosslinker for chitosan nanogel synthesis. Hyaluronic acid (HA), a biocompatible and hydrophilic polysaccharide, was used as the structural matrix for sponge scaffold fabrication [11]. Acetic acid (1% v/v) was utilised as solvent for chitosan dissolution and EDC/NHS coupling reagents were applied for optional scaffold crosslinking. All chemicals were of analytical grade and used as received without further purification. Double-distilled water was used in all preparation steps to ensure the absence of ionic impurities.

Preparation of GSH-loaded chitosan nanogels: The chitosan nanogels were prepared using an ionic gelation method. Initially, 0.5 g of chitosan was dissolved in 100 mL of 1% (v/v) acetic acid and stirred overnight to obtain a clear polymer solution. Following complete dissolution, 100 mg of reduced glutathione (GSH) was added to the chitosan solution under continuous stirring to ensure uniform incorporation [12]. Nanogel formation was induced by the dropwise addition of 0.25% (w/v) TPP solution at a TPP-to-chitosan ratio of 1:5 while maintaining vigorous stirring at 800 rpm, resulting in spontaneous ionic crosslinking. The formed nanogels were collected by centrifugation at 10,000 rpm for 15 min, washed twice with distilled water to remove residual reagents and finally resuspended for further use [13,14].

Fabrication of nanogel–HA sponge scaffolds: The HA-based sponge scaffolds were fabricated by first dissolving 2 g of hyaluronic acid (HA) in 100 mL of distilled water under continuous stirring for 6 h to obtain a uniform polymer solution. The purified GSH-loaded chitosan nanogels were then incorporated into the HA solution and mixed for an additional 2 h to achieve a homogeneous nanogel–polymer blend. The resulting mixture was transferred into molds, frozen at -80 ºC for 12-24 h and subsequently lyophilised at -50 ºC for 48 h to form porous sponge scaffolds. When required, structural reinforcement was carried out by immersing the scaffolds in an EDC/NHS crosslinking solution for 2-4 h, followed by thorough washing and a second freeze-drying cycle to ensure stability and removal of residual reagents [15,16].

Characterisation: Optical properties were analysed by UV-DRS in the 200-800 nm range using a UV-vis spectrophotometer with an integrating sphere. Functional group interactions between PVA, HA and GSH were examined by FTIR (4000-400 cm^{-1}). Thermal behaviour was evaluated using DSC in the range of 30-400 ºC at the heating rate of 10 ºC min^{-1} in nitrogen atmosphere). Surface charge and colloidal stability were determined by zeta potential measurements at 25 ºC. Hydrodynamic size distribution was analysed using dynamic light scattering (DLS) at 25 ºC with backscatter detection at 173º. The surface morphology and gel architecture were examined using SEM (JEOL JSM-IT800) after platinum sputter-coating and particle size distribution was analysed using ImageJ software. Internal structure and nanocomposite homogeneity were investigated by TEM (JEOL JEM-1010) using thin sections mounted on carbon-coated copper grids to observe dispersion and encapsulation of GSH within the HA matrix.

Swelling index: The swelling characteristics of the HA-GSH nanogel sponge scaffold were evaluated to determine its fluid absorption capacity under simulated wound conditions. Pre-weighed dried scaffold samples were used for the study. Each scaffold was placed in 15 mL of acetate buffer (pH 5.5) and maintained at 37 ºC to mimic the mildly acidic and warm physiological environment typically present in inflamed or post-surgical wounds. At predetermined time intervals (0, 5, 10, 15, 30, 45, 60 and 75 min), the samples were carefully removed from the buffer, blotted gently with filter paper to eliminate surface moisture and weighed immediately to record the swollen weight [17]. All measurements were performed in triplicate to ensure accuracy and reproducibility.

Swelling index formula:

$$\text{Swelling index (\%)} = \frac{W_s - W_d}{W_d} \times 100 \quad (1)$$

where W_d = dry weight of the scaffold, W_s = swollen weight at each time interval.

Anti-inflammatory activity

Bovine serum albumin (BSA) denaturation assay: The HA-GSH nanogel scaffold was evaluated for anti-inflammatory potential using the BSA denaturation assay. In this method, 0.45 mL of BSA was combined with 0.05 mL of HA-GSH nanogel scaffold at varying concentrations (10, 20, 30, 40 and 50 µg/mL). The pH of the mixture was adjusted to 6.3. The solution was allowed to stand at room temperature for 10 min and subsequently incubated in a water bath at 55 ºC for 30 min. Diclofenac sodium served as the standard reference drug and DMSO acted as control. After incubation, absorbance values were recorded at 660 nm using a UV-visible spectrophotometer [18]. The percentage of protein denaturation was determined using the following equation:

$$\text{Inhibition (\%)} = \frac{A_{control} - A_{sample}}{A_{control}} \times 100 \quad (2)$$

Egg albumin denaturation assay: For the egg albumin denaturation assay, 0.2 mL of fresh egg albumin was combined with 2.8 mL of 1X phosphate buffer. Varying concentrations (10, 20, 30, 40 and 50 µg/mL) of HA GSH nanogel scaffold were then added to the mixture. The pH was adjusted to 6.3. The reaction mixture was maintained at room temperature for 10 min, followed by incubation in a water bath at 55 ºC for 30 min. Diclofenac sodium served as standard reference, while DMSO was used as control. After incubation, the absorbance of the samples was recorded spectrophotometrically at 660 nm [19]. The percentage of protein denaturation was determined using eqn. 3:

$$\text{Inhibition (\%)} = \frac{A_{control} - A_{sample}}{A_{control}} \times 100 \quad (3)$$

Membrane stabilisation assay: The *in vitro* membrane stabilisation assay is a commonly employed method for assessing the membrane-stabilizing potential of both natural and synthetic compounds. This assay evaluates the ability of a test substance to protect the cell membrane from damage and prevent the leakage of intracellular components. The materials required for the assay include human red blood cells (RBCs), phosphate-buffered saline (PBS), Tris-HCl buffer (50 mM, pH 7.4), various concentrations of HA GSH nanogel scaffold (10, 20, 30, 40 and 50 µg/mL), centrifuge tubes and a UV-vis spectrophotometer [20].

Preparation of RBC suspension: Fresh human blood was collected in a sterile tube containing an anticoagulant. The sample was centrifuged at 3000 rpm for 10 min at room temperature to separate the red blood cells (RBCs) from the plasma and other components. The supernatant was discarded and the RBC pellet was washed three times with PBS. The washed cells were then resuspended in Tris-HCl buffer to prepare a 10% (v/v) RBC suspension [21].

Assay procedure: The prepared RBC suspension (1 mL) was transferred into each centrifuge tube, followed by the addition of varying concentrations of silver nanoparticles (10, 20, 30, 40 and 50 µg/mL). The contents were mixed gently and incubated at 37 ºC for 30 min. After incubation, the tubes were centrifuged at 2500 rpm for 5 min at room temperature to pellet the RBCs. The absorbance of the collected supernatant was then recorded at 560 nm using a UV-vis spectrophotometer [22]. The percentage inhibition of haemolysis was calculated using eqn. 4:

$$\text{Inhibition (\%)} = \frac{OD_{control} - OD_{sample}}{OD_{control}} \times 100 \quad (4)$$

where OD control is the absorbance of the RBC suspension without the test compound(s) and OD sample is the absorbance of the RBC suspension with the test.

Statistical analysis: All experiments were performed in triplicate and the data are presented as mean ± SD. Statistical analysis was conducted in RStudio (R v4.x) using one-way ANOVA to determine differences among treatment groups after confirming normality and homogeneity of variance. All experiments were performed in triplicate (n = 3) and the results are presented as mean ± standard deviation (SD). Statistical significance was determined using one-way analysis of variance (ANOVA) followed by Tukey's post hoc multiple comparison test. Differences were considered statistically significant at $p < 0.05$ and highly significant at $p < 0.01$.

RESULTS AND DISCUSSION

The freeze-dried HA-GSH nanogel sponge scaffold, which was successfully prepared, exhibited a uniform white appearance with a highly porous, interconnected three-dimensional structure formed during lyophilisation. The scaffold showed a lightweight and stable sponge-like morphology with smooth pore walls, indicating homogeneous incorporation of GSH-loaded nanogels within the hyaluronic acid matrix. The well-defined porosity suggests good fluid absorption, moisture retention and suitability for controlled release and wound-healing applications.

UV-DRS analysis: As shown in Fig. 1, the UV-diffuse reflectance spectrum of the HA-GSH nanogel scaffold exhibits a prominent absorption peak at approximately 280.6 nm, which is attributed to n→π* electronic transitions associated with carbonyl and carboxylate groups. This absorption region is characteristic of polysaccharide-based hyaluronic acid systems. The close correspondence of this peak with the reported absorption range of native HA (260-285 nm) indicates that the chromophoric structure of HA remains intact following nanogel incorporation and scaffold fabrication. The presence of glutathione further contributes to the spectral profile, as thiol-containing biomolecules are known to broaden or intensify absorption bands in the 260-300 nm region. This behaviour is consistent with the previously reported spectra of GSH-functionalised nanogels and antioxidant-enriched HA-

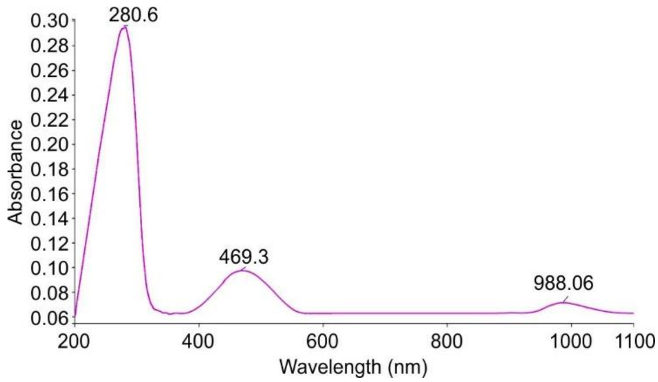

Fig. 1. UV-diffuse reflectance spectrum of HA–GSH nanogel

based materials, confirming the successful molecular integration of GSH within the polymeric matrix.

In addition to the main UV absorption, a weak shoulder observed near 469.3 nm is attributed to low-intensity visible-range light scattering rather than discrete electronic transitions. Such scattering effects are commonly reported in hydrated biopolymer nanogels and arise from microstructural heterogeneity within the polymer network. Furthermore, a broad diffuse feature centered around 988 nm appears in the near-infrared region, reflecting enhanced light scattering associated with the freeze-dried porous architecture. This NIR scattering behaviour is indicative of internal porosity, refractive index fluctuations and density gradients within the HA-GSH nanogel scaffold.

FTIR spectral studies: As shown in Fig. 2, the FTIR spectrum of the HA-GSH nanogel scaffold exhibited characteristic vibrational bands corresponding to both hyaluronic acid and glutathione, with subtle peak shifts indicating intermolecular interactions within the composite system. The broad O–H/N–H stretching band observed at 3264.81 cm^{-1} appears slightly shifted and broadened compared to pure HA (typically 3400-3200 cm^{-1}) and pure GSH (~3350-3300 cm^{-1}), suggesting enhanced intermolecular hydrogen bonding between HA hydroxyl groups, GSH amine groups and carboxyl functionalities. The C–H stretching vibration at 2930.97 cm^{-1} corresponds to the polysaccharide backbone and GSH methylene groups and shows minor positional variation relative to neat HA, indicating preservation of structural integrity without degradation. The prominent band at 1642.25 cm^{-1} (amide-I) arises from overlapping contributions of HA carboxylate C=O stretching and GSH peptide carbonyl groups; its slight shift compared to pure GSH (~1660-1650 cm^{-1}) supports the hydrogen-bond-mediated interactions rather than new covalent bond formation. Similarly, the amide II band at 1553.06 cm^{-1} confirms the presence and structural preservation of GSH within the matrix. The symmetric COO^- stretching band at 1404.32 cm^{-1}, characteristic of HA, remains intact with slight variation, suggesting electrostatic interaction between HA carboxylate groups and protonated chitosan amines. The strong absorptions in the 1307-1024 cm^{-1} region correspond to C–O–C and C–O stretching vibrations of the HA glycosidic framework, with minor intensity changes indicating modification of the hydrogen-bonding environment upon nanogel incorporation. The retention of low-frequency skeletal vibrations (816-560 cm^{-1}) further confirms preservation of the HA backbone structure. Thus, the FTIR results indicate the retention of chemical integrity and formation of a stable nanogel embedded sponge scaffold suitable for further applications.

Thermal studies: The thermal behaviour of the HA-GSH nanogel sponge scaffold was analysed using DSC, which showed two distinct thermal transitions typical of hydrated polysaccharide systems (Fig. 3). The first broad endothermic peak (30.28-130.00 ºC, peak at 90.74 ºC; ΔH = 392.14 J/g) corresponds to the loss of bound water and relaxation of the

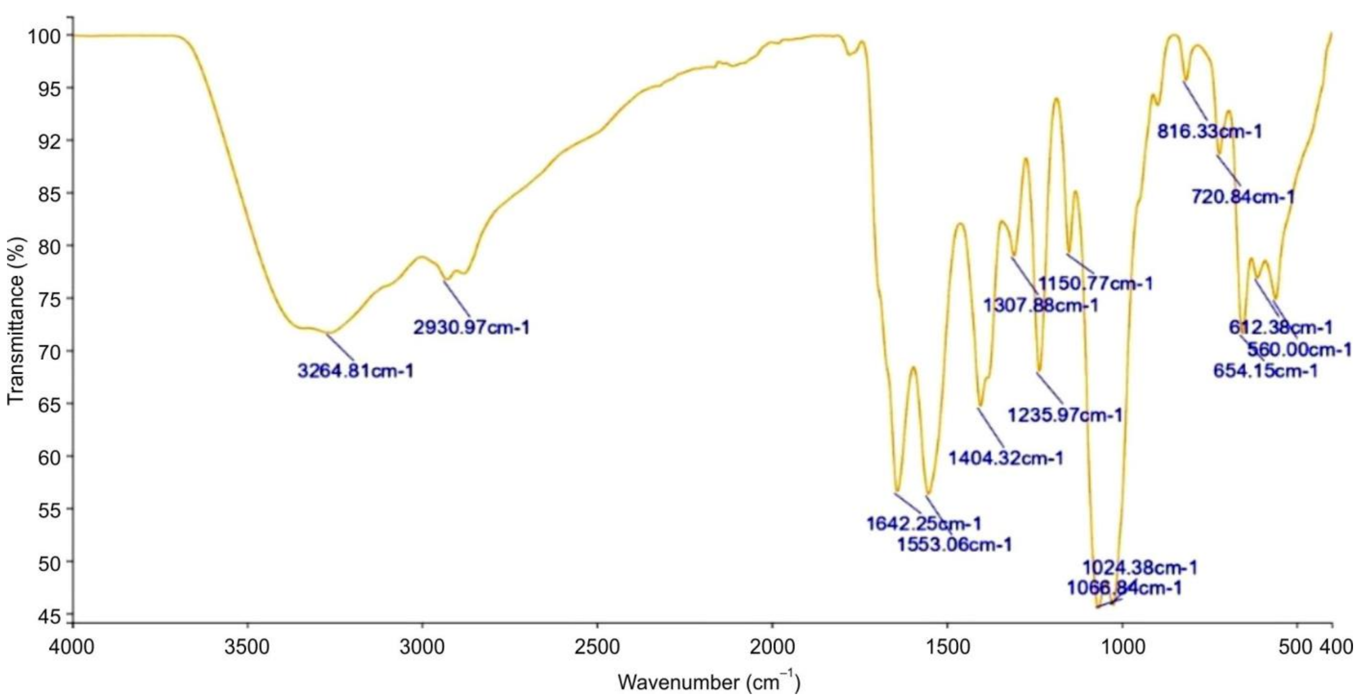

Fig. 2. FTIR spectrum of HA–GSH nanogel

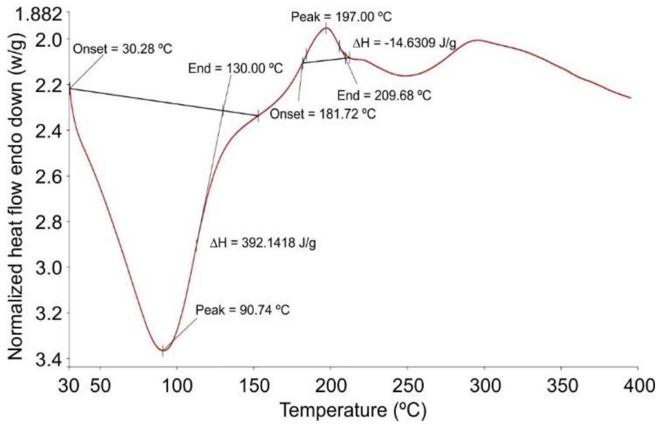

Fig. 3. DSC thermogram of HA–GSH nanogel

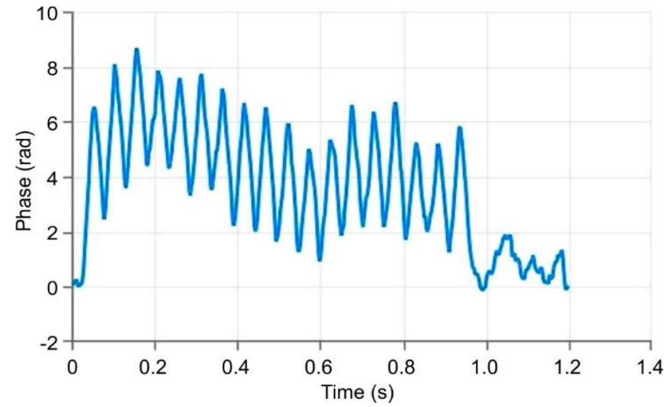

Fig. 4. Zeta potential plot of the HA–GSH nanogel

hydrated polymer network, indicating strong hydrogen bonding and high water retention. The shift of the glass transition temperature to ~90 ºC compared to pure HA suggests reduced polymer chain mobility due to interactions between HA and GSH-loaded chitosan nanogels.

A second transition at higher temperature (181.72-209.68 ºC, peak at 197.00 ºC; ΔH = -14.63 J/g) is attributed to polymer rearrangement followed by the onset of thermal degradation. The presence of this transition at elevated temperature indicates that nanogel incorporation does not compromise the thermal stability of the HA matrix. The DSC results confirm strong hydration behaviour, improved polymer–nanogel interactions and adequate thermal stability of the HA-GSH nanogel sponge.

Zeta potential: The HA-GSH nanogel exhibited a zeta potential of +26.13 mV, indicating moderate electrostatic stability in aqueous dispersion. The positive surface charge is attributed to protonated amine groups of chitosan and thiol-associated functionalities, resulting in a cationic surface. The measured conductivity of 1.713 mS cm^{-1} suggests suitable ionic strength of the dispersion medium, supporting stable particle dispersion (Fig. 4). This level of surface charge provides sufficient electrostatic repulsion, minimizing aggregation and promoting uniform nanogel distribution within the HA matrix. These results confirm adequate colloidal stability and favourable surface electrostatic properties of the HA-GSH nanogel.

Dynamic light scattering (DLS): Dynamic light scattering (DLS) analysis was performed to determine the hydrodynamic size distribution of the HA-GSH nanogel system. The Z-average hydrodynamic diameter was 211.5 nm, which falls within the typical range reported for HA-based nanogels. The size distribution exhibited a multimodal profile with a polydispersity index (PDI) of 1.0, indicating broad size distribution associated with hierarchical nanogel structures formed after freeze-drying. The dominant peak at 853.3 nm corresponds to larger nanogel assemblies formed through secondary aggregation, while smaller peaks at 87.6 nm and 10.9 nm represent primary nanoscale nanogel populations (Fig. 5). The presence of both nano- and submicron-sized particles suggests coexistence of individual nanogels and loosely associated aggregate.

Swelling index: The HA–GSH nanogel sponge scaffold exhibited two-stage swelling behaviour (Fig. 6). Initially, a rapid decrease in swollen weight within the first 5 min is attributed to the release of loosely bound surface water from macropores during equilibration. Subsequently, a gradual increase in swelling from 5 to 75 min, reaching ~1.9 g, indicates diffusion-controlled water uptake through the interconnected porous network. However, the plateau observed after the prolonged immersion indicates structural stability without pore collapse, reflecting balanced interactions between HA chains and GSH-loaded nanogels, which further demonstrating the sustained hydration with good moisture retention capacity of the HA-GSH nanogel scaffold.

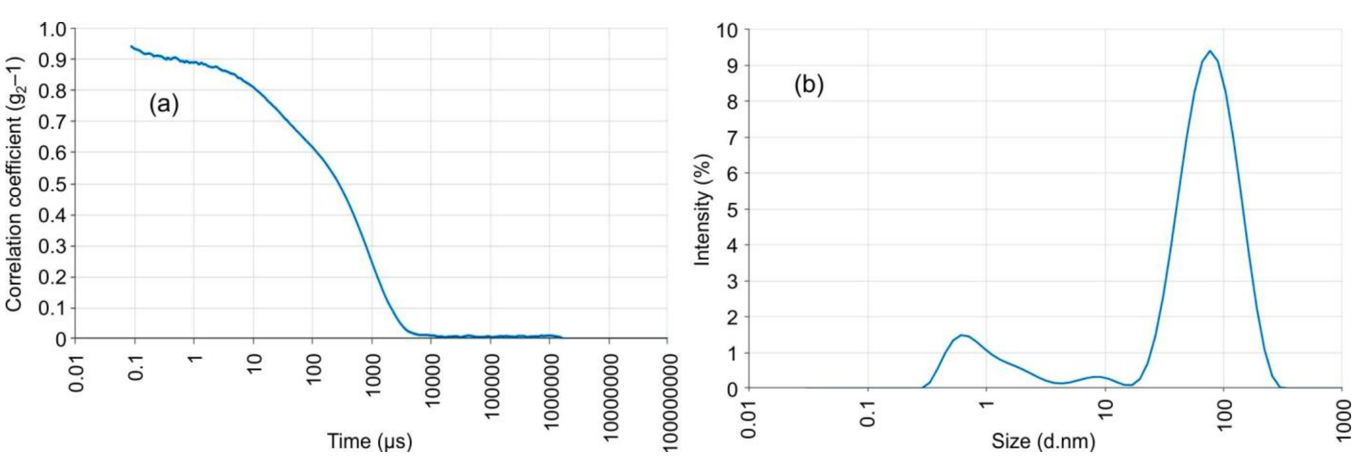

Fig. 5. DLS correlogram (a) and hydrodynamic size distribution (b) of HA–GSH nanogel

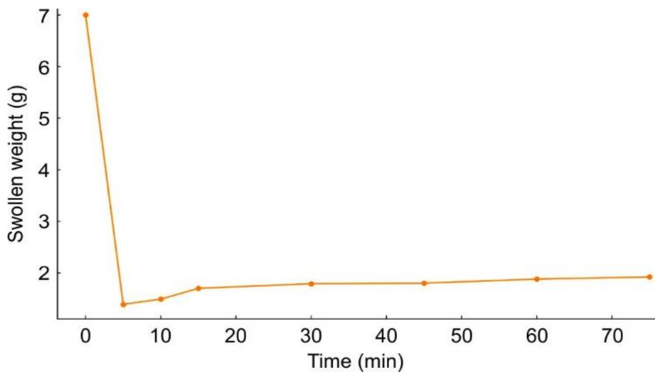

Fig. 6. Swelling profile of HA–GSH nanogel

Morphological studies: As shown in Fig. 7, the SEM micrographs of the HA-GSH nanogel sponge scaffold reveal a highly porous, interconnected 3D architecture characteristic of freeze-dried hydrogel–nanogel systems. At the lower magnification, the scaffold exhibits a continuous network of large, open macropores with irregular yet well-defined boundaries. The uniform distribution of these pores throughout the matrix confirms effective ice-templated porosity formation during the freeze-drying process. Such pore architectures are comm only reported for HA-based sponges, where controlled freezing induces phase separation and generates interconnected channels that facilitate fluid transport and mass exchange [23].

At higher magnifications, the pore walls appear smooth and continuous, with no evidence of cracking, fragmentation, or phase separation. This structural continuity indicates strong molecular compatibility between hyaluronic acid and GSH-loaded nanogels, consistent with the observations in thiolated and antioxidant-modified polysaccharide scaffolds. The presence of thin, sheet-like polymer walls bridging adjacent pore cavities further suggests effective intermolecular crosslinking within the nanogel-embedded HA matrix. These bridging features contribute to enhance the internal mechanical stability, a hallmark of well-crosslinked HA hydrogels and nanogel-reinforced sponge architectures.

In addition, nanoscale surface flutters are also observed along the pore walls, which are attributed to the distribution of embedded GSH nanogels within the HA framework. Similar nanoscale texturing has been reported in HA-thiol hybrid scaffolds, where nanogel incorporation increases surface roughness and contributes to hierarchical microstructural organisation. Notably, no collapsed regions or compressed pore domains are observed, indicating that the scaffold retains its structural integrity throughout the lyophilisation process.

The TEM micrographs (Fig. 8) of the HA-GSH nanogel system reveal spherical to quasi-spherical nanoparticles with sizes predominantly in the range of 80-500 nm. The particles exhibit relatively uniform electron-dense contrast, indicating a compact internal polymer network. Smooth surfaces and clearly defined boundaries suggest good structural uniformity and homogeneous incorporation of GSH within the HA matrix. The presence of discrete yet closely distributed nanoparticles further supports the formation of stable HA-GSH nanogels with consistent nanoscale morphology.

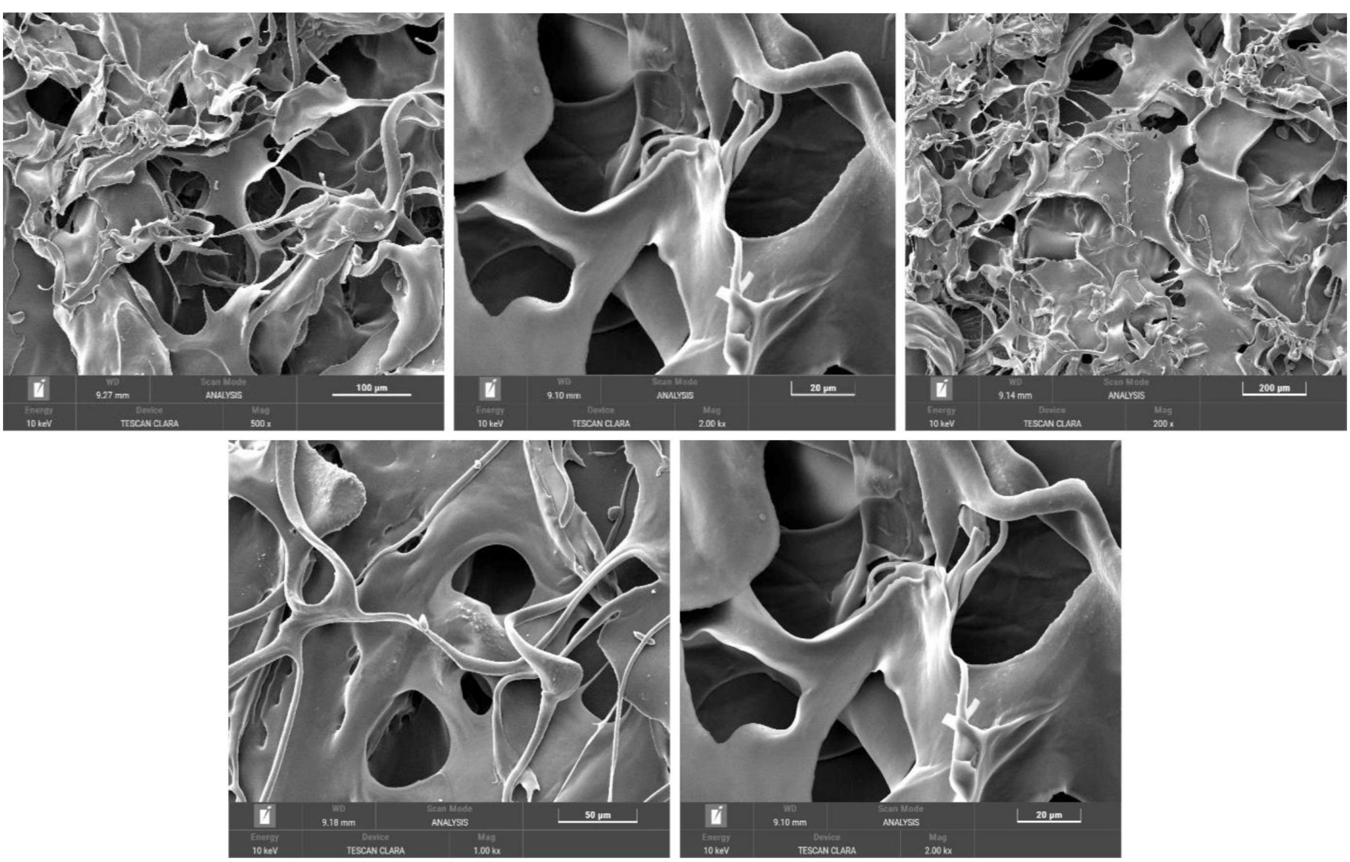

Fig. 7. SEM micrographs of HA–GSH nanogel

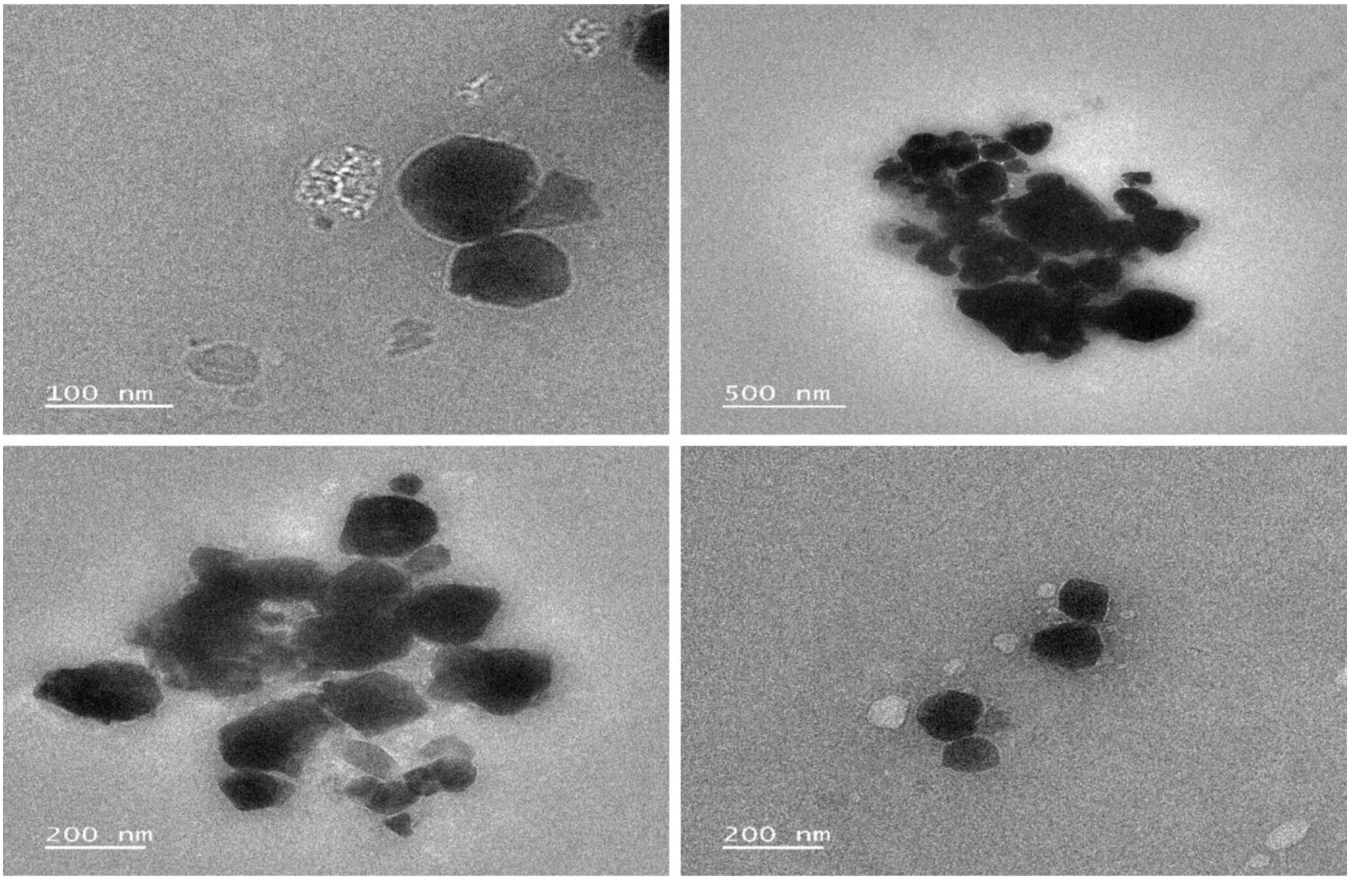

Fig. 8. TEM micrographs of HA–GSH nanogel

In some regions, mild particle clustering is observed, which can be attributed to hydrogen bonding, surface adhesion forces and residual moisture commonly associated with soft hydrogel nanogels. This limited aggregation does not indicate instability but reflects the flexible nature of hydrogel-based nanoparticles. The absence of collapsed or irregular structures, along with clear particle boundaries, confirms the preservation of the nanogel architecture during preparation and freeze-drying.

In vitro evaluation

Anti-inflammatory test

BSA denaturation assay: The BSA protein denaturation assay demonstrated that the HA-GSH nanogel scaffold exhibits concentration-dependent anti-inflammatory activity. The inhibition of protein denaturation increased from approximately 38% at 10 μg/mL to about 73% at 50 μg/mL, indicating effective protection against heat-induced protein unfolding (Fig. 9). This behaviour can be attributed to hydroxyl and thiol functionalities of the HA-GSH system, which contribute to protein stabilisation [24].

Comparison with the standard drug showed slightly higher inhibition values (≈82-85% at 50 μg/mL); however, the HA-GSH nanogel scaffold approached comparable activity at higher concentrations. The progressive increase in inhibition suggests formation of a protective hydration environment around protein molecules, reducing aggregation and thermal denaturation. Hence, these results confirm that the HA-GSH nanogel scaffold possesses notable protein-stabilizing and antidenaturation capability, supporting its potential for anti-inflammatory and wound-healing applications [19].

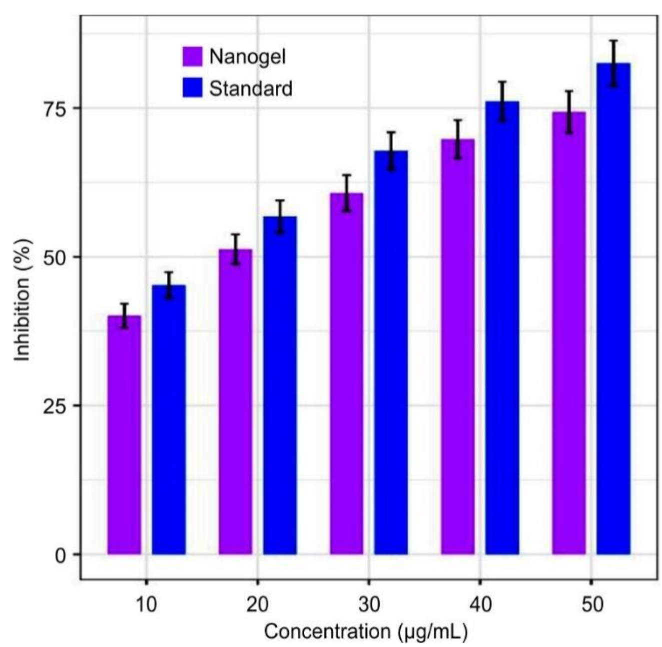

Fig. 9. Concentration-dependent inhibition of bovine serum albumin (BSA) denaturation by the HA–GSH nanogel

Egg albumin denaturation assay: The egg albumin denaturation assay demonstrated that the HA-GSH nanogel scaffold exhibits dose-dependent anti-inflammatory activity. The percentage inhibition increased from approximately 45% at 10 μg/mL to about 73% at 50 μg/mL, indicating enhanced protection against heat-induced protein denaturation at higher concentrations (Fig. 10). This behaviour is attributed to the combined effect of hydroxyl-rich HA chains and thiol groups of glutathione, which help stabilise protein structure.

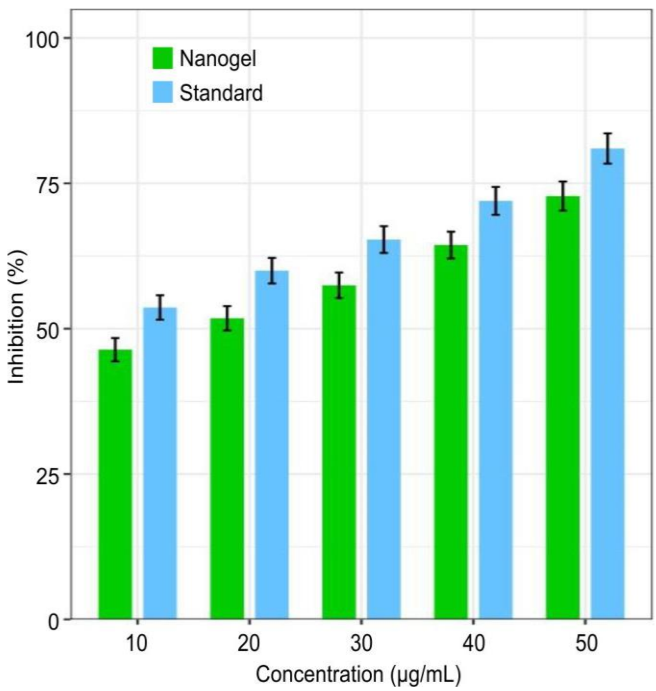

Fig. 10. Dose-dependent inhibition of egg albumin denaturation by the HA–GSH nanogel

The standard drug showed slightly higher inhibition (about 5-10% greater) across all concentrations; however, the HA-GSH nanogel displayed a steady increase in activity and approached comparable inhibition at higher doses (40-50 μg/mL). The observed effect is associated with the hydrated polymeric matrix and antioxidant activity of GSH, which reduce protein aggregation and preserve conformational stability [7,25].

Membrane stabilisation assay: The membrane stabilisation assay demonstrated that the HA-GSH nanogel scaffold exhibits concentration-dependent protection against heat-induced hemolysis. The percentage inhibition increased from ~50% at 10 μg/mL to nearly 83% at 50 μg/mL, indicating effective prevention of erythrocyte membrane lysis (Fig. 11). This behaviour is attributed to hydrogen bonding, hydration layer formation and thiol-mediated stabilisation associated with the HA-GSH system.

The standard drug showed slightly higher inhibition, reaching about 90% at 50 μg/mL; however, the nanogel scaffold closely approached comparable activity at higher concentrations (40-50 μg/mL). The enhanced protection is due to the combined effect of the HA hydration shell and antioxidant activity of GSH, which reduce membrane damage and oxidative stress and confirm significant anti-inflammatory potential of the HA-GSH nanogel scaffold and support its suitability for wound-healing applications [19,21].

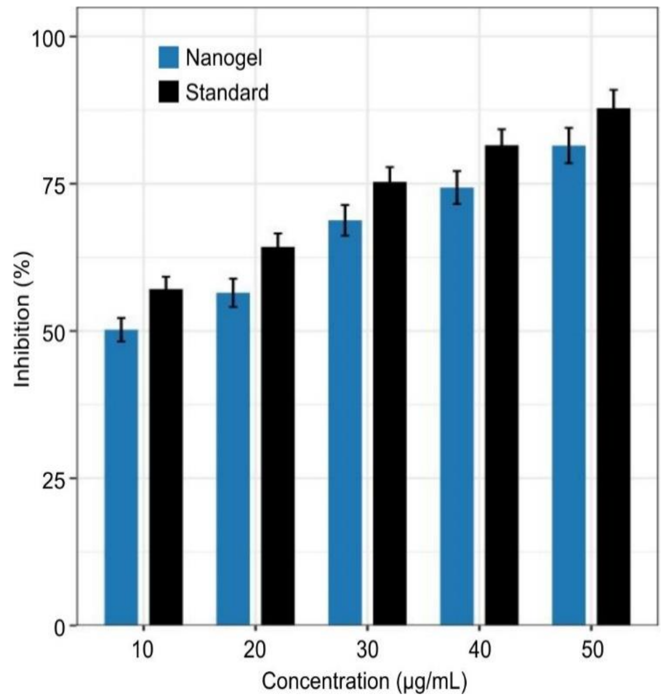

Fig. 11. Concentration-dependent membrane stabilisation activity of the HA–GSH nanogel

Conclusion

In this study, a hyaluronic acid (HA) based sponge scaffold incorporating glutathione (GSH) loaded chitosan nanogels was successfully developed using ionic gelation followed by freeze drying. The resulting HA-GSH nanogel sponge exhibited a highly porous, interconnected 3D architecture with uniform pore distribution, well-defined nanoscale GSH-loaded particles and a positively shifted zeta potential indicative of colloidal stability. Comprehensive physico-chemical characterisation using UV-DRS, FTIR and DSC confirmed the preservation of key functional groups, favourable polymer-nanogel interactions and satisfactory thermal stability, while DLS, SEM and TEM analyses demonstrated homogeneous nanogel dispersion within the HA matrix. Functionally, the scaffold displayed a controlled and progressive swelling profile, supporting sustained moisture retention suitable for exudetive wound environments. *In vitro* anti-inflammatory evaluation including bovine serum albumin and egg albumin denaturation assays as well as red blood cell membrane stabilisation, revealed a clear concentration-dependent inhibitory response, with higher nanogel concentrations approaching the activity of the reference drug. These results demonstrate that integration of GSH-loaded chitosan nanogels within an HA scaffold yields a unified platform capable of providing structural support, hydration and effective anti-inflammatory action key requirements for advanced wound-healing materials.

ACKNOWLEDGEMENTS

The authors sincerely acknowledge Saveetha Institute of Medical and Technical Sciences (SIMATS), Chennai, for providing the laboratory facilities, research support and infrastructure required to carry out this work.

CONFLICT OF INTEREST

The authors declare that there is no conflict of interests regarding the publication of this article.

DECLARATION OF AI-ASSISTED TECHNOLOGIES

During the preparation of this manuscript, the authors used an AI-assisted tool(s) to improve the language. The authors reviewed and edited the content and take full responsibility for the published work.

REFERENCES

1. Z. Zhao, X. Zheng, Y. Li, X. Yao, H. Wang and X. Song, *Adv. Funct. Mater.*, 34, 2409050 (2024); https://doi.org/10.1002/adfm.202409050
2. G.N. Iaconisi, P. Lunetti, N. Gallo, A.R. Cappello, G. Fiermonte, V. Dolce and L. Capobianco, *Int. J. Mol. Sci.*, **24**, 10296 (2023); https://doi.org/10.3390/ijms241210296
3. S.K. Georgiou-Siafis and A.S. Tsiftsoglou, *Antioxidants*, **12**, 1953 (2023); https://doi.org/10.3390/antiox12111953
4. A.C. Lima, R.L. Reis, H. Ferreira and N.M. Neves, *ACS Biomater. Sci. Eng.*, **7**, 3229 (2021); https://doi.org/10.1021/acsbiomaterials.1c00412
5. R. Jeyavelkumaran, S. Harikrishnan, M. S. Dhanapal, N. Keerthivasan, and S. Valliappan, *Pept. Sci.*, **118**, e70027 (2026); https://doi.org/10.1002/pep2.70027
6. Y. Wang, X. Lou, L. Yang and Y. Hou, *Curr. Pharm. Des.*, **31**, 1247 (2025); https://doi.org/10.2174/0113816128347060241105032329
7. R. Jeyavelkumaran, P. Panneerpandian, S. Panneerselvam, R. Muthu and S.H. Jahir, *Regen. Eng. Transl. Med.*, (2025); https://doi.org/10.1007/s40883-025-00522-w
8. J. Grenier, H. Duval, P. Lv, F. Barou, C. Le Guilcher, R. Aid, B. David and D. Letourneur, *Biomater. Adv.*, **139**, 212973 (2022); https://doi.org/10.1016/j.bioadv.2022.212973
9. N. Salari, K. Mansouri, E. Valipour, M. Jaymand, S. Rasoulpoor, F. Abam, S. Dokaneheifard and M. Mohammadi, *Daru*, **29**, 439 (2021); https://doi.org/10.1007/s40199-021-00416-6
10. R. Muthu, R. Jeyavelkumaran and M. Mohan, *BioNanoSci.*, **16**, 237 (2026); https://doi.org/10.1007/s12668-026-02440-9
11. F. Sami El-banna, M.E. Mahfouz, S. Leporatti, M. El-Kemary and N. A. N. Hanafy, *Appl. Sci.*, **9**, 2193 (2019); https://doi.org/10.3390/app9112193
12. N.H. Hoang, T. Le Thanh, R. Sangpueak, J. Treekoon, C. Saengchan, W. Thepbandit, N.K. Papathoti, A. Kamkaew and N. Buensanteai, *Polymers*, **14**, 662 (2022); https://doi.org/10.3390/polym14040662
13. N. Van Bavel, T. Issler, L. Pang, M. Anikovskiy and E.J. Prenner, *Molecules*, **28**, 4328 (2023); https://doi.org/10.3390/molecules28114328
14. A. Mustafa, M. ArumughamIndiran, E. Perumal, A. Ponnala, D.A. Rasheed, K. Ramalingam, R. Shanmugham and M.I. Karobari, *Naunyn Schmiedebergs Arch. Pharmacol.*, **398**, 15335 (2025); https://doi.org/10.1007/s00210-025-04185-w
15. S.M. Davachi, S.M.A. Haramshahi, S.A. Akhavirad, N. Bahrami, S. Hassanzadeh, S. Ezzatpour, N. Hassanzadeh, M. Khanmohammadi, M.M. Kebria, and Z. Bagher, *Mater. Today Commun.*, **30**, 103230 (2022); https://doi.org/10.1016/j.mtcomm.2022.103230
16. Z. Nabizadeh, M. Nasrollahzadeh, F. Heidari and D. Nasrabadi, *Int. J. Biol. Macromol.*, **283**, 137314 (2024); https://doi.org/10.1016/j.ijbiomac.2024.137314
17. A.K. Moussa, H.A. Abd El-Rahman, R.R. Mohamed and D.H. Hanna, *Biomacromolecules*, **26**, 3495 (2025); https://doi.org/10.1021/acs.biomac.5c00126
18. R. Shanmugam, M. Tharani, S.S. Abullais, S.R. Patil and M.I. Karobari, *BMC Complement. Med. Ther.*, **24**, 241 (2024); https://doi.org/10.1186/s12906-024-04552-9
19. S. Balasubramaniyam, T. Rathinam, M. Srinivasan, P. Arulselvan, S. Mickymaray and F.A. Alfaiz, *3 Biotech*, **15**, 358 (2025); https://doi.org/10.1007/s13205-025-04526-9
20. K. Pandi, B.V. Cheriyan, D. Pandu, A. Badhurudeen, S.S. Gunasekaran, S.K. Manivannan, P. Loganathan, J. Ramasamy, Y. Shanmugam and M.S. Kannuchamy, *J. Natural Remedies*, **25**, 2773 (2005); https://doi.org/10.18311/jnr/2025/50258
21. K. Akash, A.J.P. Winston, K.M. Mohamed, P. Sagayaraj, J. Madhavan, S.R. Kumar, S.A. Jayanthi and J.J. Vijaya, *Inorg. Chem. Commun.*, **169**, 113046 (2024); https://doi.org/10.1016/j.inoche.2024.113046
22. M. Mahalingam, D.S. Pillai and R.K. Shanmugam, *J. Indian Acad. Oral Med. Radiol.*, **36**, 278 (2024); https://doi.org/10.4103/jiaomr.jiaomr_43_24
23. F. Zhang, C. He, L. Cao, W. Feng, H. Wang, X. Mo and J. Wang, *Int. J. Biol. Macromol*., **48**, 474 (2011); https://doi.org/10.1016/j.ijbiomac.2011.01.012
24. S.S. Myint, C. Laomeephol, S. Thamnium, S. Chamni and J.A. Luckanagul, *Pharmaceutics*, **15**, 2671 (2023); https://doi.org/10.3390/pharmaceutics15122671
25. Z. Xu, G. Liu, P. Liu, Y. Hu, Y. Chen, Y. Fang, G. Sun, H. Huang and J. Wu, **147**, 147 (2022); https://doi.org/10.1016/j.actbio.2022.05.047